

## A Metamaterial-Inspired Sensor for Combined Inductive-Capacitive Detection

Long, J.; Wang, B.

TR2015-014 February 24, 2015

### Abstract

In this letter, we introduce a metamaterial-inspired sensor that is capable of performing combined inductive-capacitive sensing, so that both detection and discrimination between metallic and dielectric objects are accomplished. Metals and dielectrics are distinguished based on their different responses to inductive and capacitive sensing. Both sensing modes are integrated into a single sensing unit, which is developed from an Omega-shaped metamaterial structure. Inductive and capacitive sensing are simultaneously realized when the sensor is operated at off-resonant frequencies. The proposed sensor is fabricated and experimented with metallic and dielectric objects. The measurement results demonstrate the proposed sensor's ability of conducting combined sensing with a range of 10 mm. The performance of proposed sensor is competitive among industrial state-of-the-art proximity sensors, yet with added functionality of differentiating metallic and dielectric objects.

*Applied Physics Letters*

© 2015 MERL. This work may not be copied or reproduced in whole or in part for any commercial purpose. Permission to copy in whole or in part without payment of fee is granted for nonprofit educational and research purposes provided that all such whole or partial copies include the following: a notice that such copying is by permission of Mitsubishi Electric Research Laboratories, Inc.; an acknowledgment of the authors and individual contributions to the work; and all applicable portions of the copyright notice. Copying, reproduction, or republishing for any other purpose shall require a license with payment of fee to Mitsubishi Electric Research Laboratories, Inc. All rights reserved.



# A Metamaterial-Inspired Sensor for Combined Inductive-Capacitive Detection

Jiang Long<sup>1,2, a)</sup> and Bingnan Wang<sup>1, b)</sup>

<sup>1)</sup>Mitsubishi Electric Research Laboratories, 201 Broadway, Cambridge, MA, 02139 USA

<sup>2)</sup>University of California, San Diego, 9500 Gilman Dr., La Jolla, CA, 92093 USA

In this letter, we introduce a metamaterial-inspired sensor that is capable of performing combined inductive-capacitive sensing, so that both detection and discrimination between metallic and dielectric objects are accomplished. Metals and dielectrics are distinguished based on their different responses to inductive and capacitive sensing. Both sensing modes are integrated into a single sensing unit, which is developed from an  $\Omega$ -shaped metamaterial structure. Inductive and capacitive sensing are simultaneously realized when the sensor is operated at off-resonant frequencies. The proposed sensor is fabricated and experimented with metallic and dielectric objects. The measurement results demonstrate the proposed sensor's ability of conducting combined sensing with a range of 10 mm. The performance of proposed sensor is competitive among industrial state-of-the-art proximity sensors, yet with added functionality of differentiating metallic and dielectric objects.

Proximity sensing techniques have been developed for many years<sup>1-12</sup>. Nowadays, owing to the great significance to many industrial applications, there tends to be a great demand on not only sensing the approaching of the objects, but also discriminating between metals and dielectrics. For instance, an automatic drilling machine uses such sensors for intelligently detecting and distinguishing metallic and nonmetallic parts so as to avoid unexpected damages of the drilling bits. Also, next generation car intelligence wants to know whether a man or some other type of cargo is on the car seat so that the passengers can be better protected. Moreover, robots and bio-sensing are also potential applications. Therefore, it is desirable for proximity sensors to incorporate the new function to distinguish metals and dielectrics.

Neither conventional capacitive or inductive sensing technique can realize the differentiation by itself. Thanks to the peculiar conductive property of a metallic object, it induces both inductive and capacitive sensing, whereas a dielectric object responds only to the capacitive sensing. It is, thus, possible to sense and distinguish the two types of materials with the combined inductive-capacitive sensing technique. By simply combining the two inductive and capacitive sensor devices together, metal and dielectric can be distinguished<sup>3,13</sup>. However, it requires twice area as a single inductive or capacitive sensor. Alternating even and odd modes to excite a coil has been reported for integrating inductive and capacitive sensors<sup>4</sup>. Nevertheless, the proposed method needs two sets of coils, one for excitation and the other for signal reception. Besides, frequently switching for excitation and detection system is required to work on the two different modes, which still complicates the detection circuitry. Therefore, a type of sensor that combines inductive and capacitive sensing with compactness and simplicity is needed.

This letter introduces a combined inductive-capacitive sensor inspired by metamaterial (MTM) sensors<sup>5-8</sup>. The

basic principle of conventional MTM sensors is to detect the change in resonant frequency due to the disturbance to the near field electric/magnetic components caused by the presence of an object. They are typically incapable of achieving combined inductive-capacitive sensing. It is also well known that MTMs present either inductive or capacitive properties at their upper or lower band instead of the resonant frequency. This inspires us to utilize the off-resonance responses of the sensor to achieve both inductive and capacitive sensing, so that metals and dielectrics can be distinguished. In addition, since both sensing techniques are included in a single structure, the proposed sensor can provide extra size reduction and also further simplification in detecting circuitry.

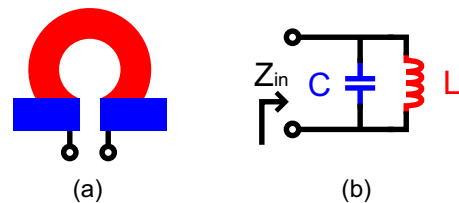


FIG. 1.  $\Omega$ -shape metamaterial unit cell and its equivalent circuit around resonance

To demonstrate the proposed combined sensing, an  $\Omega$ -shaped unit cell structure is initially adopted<sup>14,15</sup> as the sensor, as illustrated in Fig. 1. It is easy to understand that its circuitry equivalence is a shunt  $LC$  resonance, where  $L$  stems from the long arc-shape ring (the red part of the structure), and  $C$  comes from the two horizontally placed short bars (the blue parts). The input admittance can be expressed as

$$Y_{in} = j \left( \omega C - \frac{1}{\omega L} \right), \quad (1)$$

so the reflection coefficient of the single-port network is

$$S_{11} = \frac{Y_0 - Y_{in}}{Y_0 + Y_{in}} = \frac{0.02 - j \left( \omega C - \frac{1}{\omega L} \right)}{0.02 + j \left( \omega C - \frac{1}{\omega L} \right)}, \quad (2)$$

<sup>a)</sup>Work done when author was with Mitsubishi Electric Research Laboratories.

<sup>b)</sup>e-mail: bwang@merl.com

and thus, its phase (in degrees) is expressed as

$$\phi = \angle S_{11} = -\frac{360}{\pi} \arctan\left(\frac{\omega C - \frac{1}{\omega L}}{0.02}\right) \text{ (degrees)}. \quad (3)$$

From Eq. 3, it can be seen that  $\phi$  is reversely proportional to  $C$  and  $L$  but with different coefficients, so their contributions to  $\phi$  are different. When a metallic object gets close to the sensor, increase in  $C$  (due to the material polarization) and decrease in  $L$  (due to the induced eddy currents) occur. By contrast, if the object is dielectric, only the increase in  $C$  can be found, because no eddy currents are induced. Consequently, different types of objects have unequal impacts to  $Y_{in}$  and  $\phi$ . If only the change in the resonant frequency of the input admittance  $Y_{in}$  is monitored, as what is usually measured in the conventional MTM sensors<sup>5–8</sup>, it can only detect the proximity of the objects, but fails in distinguishing the type of the targets. By contrast, if  $Y_{in}$  at two frequencies are measured, then the contributions from  $C$  and  $L$  are clear, which enables us to discriminate between metallic and dielectric approaching objects. Therefore, by capturing the changes in  $\phi$  of the  $\Omega$ -shaped sensor at two frequencies, the approaching metal or dielectric can be detected and distinguished.

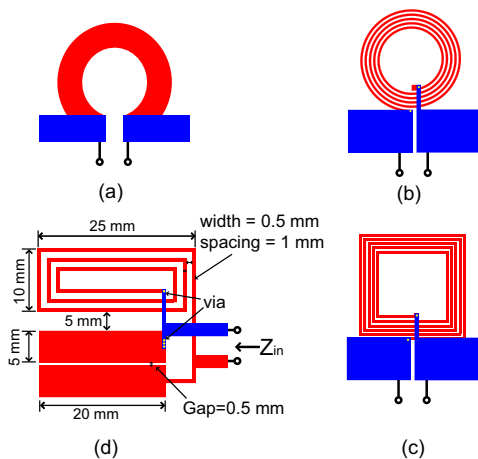


FIG. 2. Evolution of the sensor structure from  $\Omega$ -shape meta-material unit cell. The design starts from the original  $\Omega$ -shape structure (a), and then it is replaced with a circular coil and rectangular patches (b), transformed to square coil (c), and rearranged the relative position of the coil and patch (d), which is the final design. The red and blue colors represent the top and bottom layers, respectively. The detailed dimensions of the final design are labeled in (d).

Identifying the inductive and capacitive contributions of a resonant structure is helpful, as it not only explains the principle of the combined sensing technique, but also is essential to manipulating the operating frequency and the geometry of the sensor. In practice, different resonant structures can be developed based on the MTM unit cells by modifying the geometrical designs, so that desired resonant frequency is achieved while the physical size and

shape of the sensor are maintained. Fig. 2 shows how the sensing structure is developed from an initial  $\Omega$ -shaped structure. The arc-shape inductive part can be replaced with spiral structure, so that the inductance is increased and the resultant resonant frequency is decreased. The two short bars in the  $\Omega$ -shaped structure, which form the capacitor, are extended in order to increase the capacitance. As the two parts contribute to inductance and capacitance respectively, they can be modified separately and arranged in a manner based on the geometrical requirements of the sensing application. As an example, we designed a sensing structure as shown in Fig. 2(d), which resonates at 200 MHz. The inductive part is composed of a square spiral with a dimension of 25 mm  $\times$  10 mm, a wire width of 0.5 mm, and a spacing between wires of 1 mm. The capacitive part is formed by a coplanar capacitor, composed of two rectangular patches of 20 mm  $\times$  5 mm each, with a gap of 0.5 mm between them. The two parts are placed in parallel with a spacing of 5 mm. The overall size that the whole sensor is about 30 mm  $\times$  30 mm, about  $0.05\lambda_0 \times 0.05\lambda_0$  ( $\lambda_0$  is the free space wavelength at 500 MHz, the highest frequency used in the measurement).

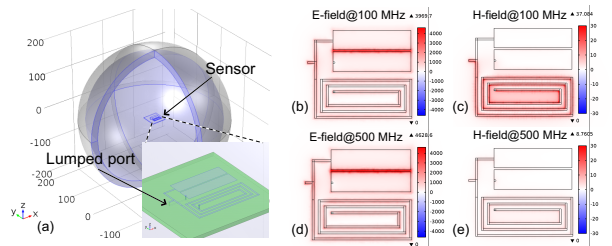


FIG. 3. (a) Numerical model of the sensor in COMSOL. Simulated (b) electric and (c) magnetic field distribution at 100 MHz; (d) electric and (e) magnetic field distribution at 500 MHz.

Fig. 3(a) shows the simulation model with COMSOL Multiphysics with the sensor structure built in the middle of a spherical domain confined by a perfect matching layer. The sensor is built on an 1.6-mm-thick FR4 substrate ( $\epsilon_r = 4.5$ ) with geometry depicted in Fig. 2(d). The electric and magnetic fields distribution around the sensing structure is simulated at 100 MHz (below resonance) and 500 MHz (above resonance), and shown in Fig. 3(b) to (e), respectively. The magnetic field at 100 MHz (Fig. 3(c)) is significantly higher around the spiral structure, indicating the structure is inductive. Whereas at 500 MHz, the electric field distribution (Fig. 3(d)) is more concentrated on the patches, indicating a capacitive feature. The simulation result confirms our theoretical predictions.

The sensor was fabricated using standard printed circuit board technology, which is shown in Fig. 4(a)-(c). Three types of structures are fabricated: (a) with both inductive and capacitive components; (b) with only inductive component; (c) with only capacitive component. To identify the inductive and capacitive properties for

each parts, the samples shown in Fig. 4(b) and (c) are measured and modeled with lumped elements, respectively. Once again, it shows the functionalities of the inductive and capacitive components, as indicated in the simulation (Fig. 3). The effective inductance and capacitance are extracted from the measurements and the lumped circuit models are built. These parameters are then used to build a circuit model for the entire combined sensor as illustrated in the inset of Fig. 4(d). The phase of the reflection coefficient for the circuit model, the measured entire sensor sample, and the EM simulation are compared in Fig. 4(d). The matched results verify our theory and EM simulation, implying that the resonant structure can be regarded as the combination of the two individual inductive and capacitive parts, which can perform inductive and capacitive sensing. From Fig. 4(d), we can also see that the resonant frequency is about 190 MHz, where the reflected phase crosses zero. Therefore, in order to realize combined sensing, two frequencies, one below 190 MHz, and another above it, are needed for measurement. In the following measurements, 100 MHz and 500 MHz are used.

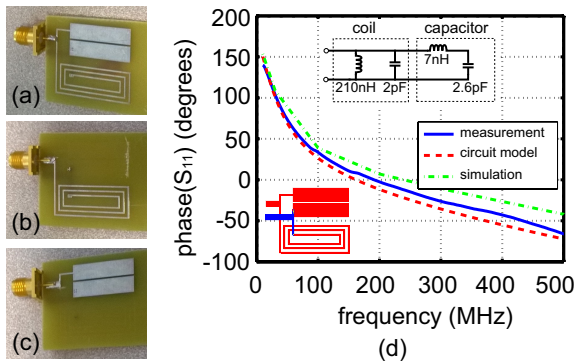


FIG. 4. Unloaded sensor and its equivalent circuit model. Three fabricated sensors, including the entire sensor (a), only the inductive part (b), and only the capacitive part (c), are measured. Based on the separate element, a circuit model is obtained and shown in the inset of (d). The experiment measurement, COMSOL simulation and result from the derived circuit model are compared in (d).

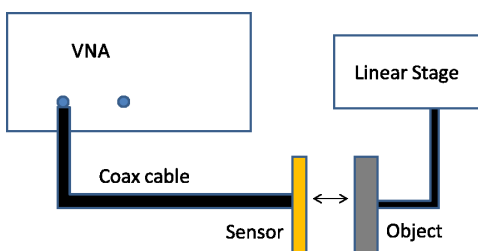


FIG. 5. Experiment setup. Reflection phase is measured with VNA while the distance between sensor and target is tuned linearly.

Fig. 5 shows the experiment setup. Aluminum and

wood blocks (relative permittivity  $\epsilon_r \approx 2$ , loss tangent  $\tan \delta \approx 0.02$ ) are used as target objects to test the performance of sensors, placed in parallel to the sensor's surface with varying distance from 2 to 20 mm. The phases of  $S_{11}$  at around 100 MHz and 500 MHz were measured with a vector network analyzer (VNA, Agilent N5230A) connected to the sensor. The measured results are summarized in Fig. 6. Fig. 6(a) and (b) exhibit the phase of  $S_{11}$  versus frequency in a small bandwidth for the cases of the object with different distances to the sensor. Specifically, Fig. 6(a) corresponds to the phase change near 100 MHz due to the slab of aluminum, whereas Fig. 6(b) is the results centered at 500 MHz for the proximity of the wood object. Clear phase shifts can be identified when the object approaches within 20 mm, and the closer the object is the more phase shift is observed. The phases around 100 MHz for wood and 500 MHz for the metal are not presented because they are not of interest. To further show the relationship between the distance of the wood or aluminum object, the phase of  $S_{11}$  at two frequency points, 100 and 500 MHz, versus the distance due to different material approaching are plotted in Fig. 6(c) and (d), respectively. They show that at low frequency the sensor is inductive, only metal induces change of  $S_{11}$ ; the sensor does not response to dielectric materials (see Fig. 6(c)). By contrast, capacitive sensing occurs at 500 MHz, so the sensor responses to both wood and aluminum as discussed above. This clearly demonstrates the ability of sensing and distinguishing between metallic and nonmetallic objects. In addition, as can be seen from Fig. 6(c), the inductive sensing causes  $33^\circ$  to  $46.7^\circ$  phase change, whereas Fig. 6(d) exhibits  $-67.2^\circ$  to  $-68.8^\circ$  change due to capacitive sensing. For both sensing modes, the sensitivity of the phase change to the distance decreases as distance increases. If the minimum detectable phase change is  $0.1^\circ$ <sup>16</sup>, then the maximum sensing range of the combined sensor for both types of objects is at least 10 mm. It should be noted that the sensitivity of the phase change is determined by the ratio of the capacitance change due to the proximity of the dielectric object to the intrinsic capacitance of the sensor, which can be further improved by optimizing sensor design with lower intrinsic capacitance.

The performance of the proposed sensor is compared with the state-of-art capacitive and inductive proximity sensors. The specifications of major products including nominal sensing range  $S_n$  and dimensions are obtained from data sheets<sup>17-20</sup>. The actual sensing range is adjusted by a correction factor for specific materials (i.e., wood and aluminum)<sup>9,10</sup>. The dimension  $D_{eff}$  is corrected as the geometric mean of the two dimensions of the sensing plane. As the sensing range is generally proportional to the dimension<sup>11,12</sup>, we chose the ratio of sensing range to sensor dimension,  $S_n/D_{eff}$ , as a figure-of-merit (FOM) for performance comparison. The FOM of the proposed sensor and all referred commercially available industrial sensors are presented in Fig. 7, from which it can be seen that the proposed combined sensor has a sensing range

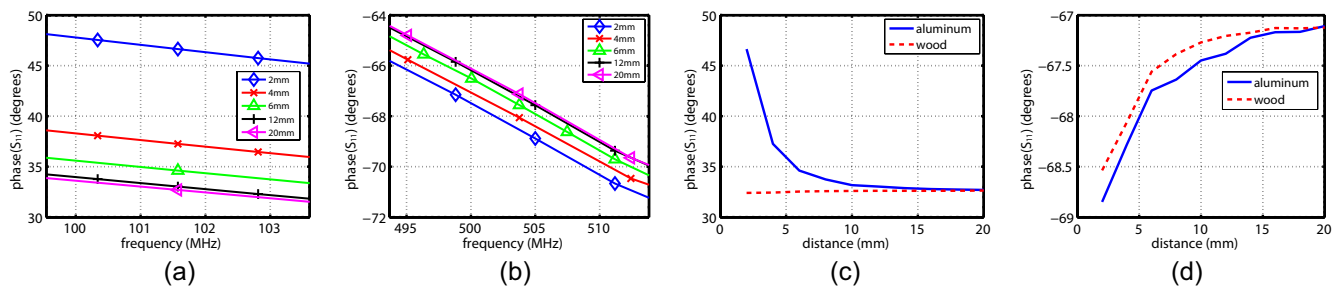


FIG. 6. Measured phase of  $S_{11}$ . (a) phase response around 100 MHz with aluminum approaching; (b) phase response around 500 MHz with wood approaching; (c) phase change at 100 MHz versus the distance of the object; (d) phase change at 500 MHz versus the distance of the object.

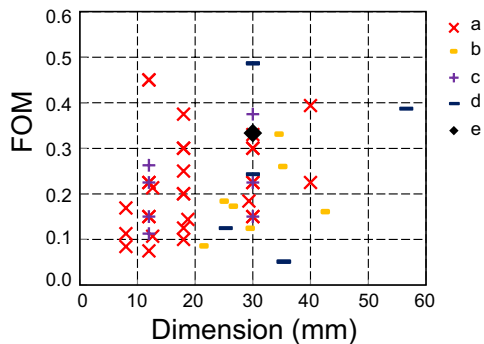


FIG. 7. Comparison with state-of-the-art proximity sensor. a: AutomationDirect sensors (V, CR, CM, CT, CK series)<sup>17</sup>; b: OMRON sensors (E2E, E2B, E2K-X series)<sup>18</sup>; c: IFM sensors (Tubular M12, M18, M30 series)<sup>19</sup>; d: SICK sensors (IMA, IQ Flat, CQ series)<sup>20</sup>; e: This work.

comparable to existing inductive and capacitive sensors, and has the additional capability of distinguishing metallic and dielectric objects.

In summary, this paper reports a MTM-inspired combined inductive-capacitive sensing method for detecting and distinguishing metallic and non-metallic objects. Metallic and dielectric objects can be distinguished by measuring both of their inductive and capacitive responses based on the fact that they respond differently to inductive and capacitive sensing. Both inductive and capacitive sensing are simultaneously realized when the sensor is operating at off-resonant frequencies. The proposed method is demonstrated with typical printed circuit board technology. The designed sensor can distinguish the metallic and dielectric objects with a sensing range about 10 mm, showing a competitive performance compared with commercially available industrial proximity sensors.

<sup>1</sup>D. Tumpold and A. Satz. Contactless seat occupation detection system based on electric field sensing. In *Industrial Electronics, 2009. IECON '09. 35th Annual Conference of IEEE*, pages 1823–1828, Nov 2009.

<sup>2</sup>Hubert Zangl. Capacitive sensors uncovered: Measurement, detection and classification in open environments. *Procedia Engineering*, 5(0):393 – 399, 2010.

<sup>3</sup>Mikihiro Yamashita and Kaoru Furukawa. Electronic detector with capacitor sensor and magnetic field sensor for locating an object behind a wall surface, 1989.

<sup>4</sup>B. George, H. Zangl, T. Bretterkieber, and G. Brasseur. *Instrumentation and Measurement, IEEE Transactions on*, (5):1463–1470, May 2008.

<sup>5</sup>Ibraheem A. Ibraheem Al-Naib, Christian Jansen, and Martin Koch. Thin-film sensing with planar asymmetric metamaterial resonators. *Applied Physics Letters*, 93(8):–, 2008.

<sup>6</sup>Rohat Melik, Emre Unal, Nihan Kosku Perkgoz, Christian Puttlitz, and Hilmi Volkan Demir. Flexible metamaterials for wireless strain sensing. *Applied Physics Letters*, 95(18):–, 2009.

<sup>7</sup>Jordi Naqui, Miguel Durán-Sindreu, and Ferran Martín. Novel sensors based on the symmetry properties of split ring resonators (SRRs). *Sensors*, 11(8):7545–7553, 2011.

<sup>8</sup>W. Withayachumnankul, K. Jaruwongrungrsee, C. Fumeaux, and D. Abbott. Metamaterial-inspired multichannel thin-film sensor. *Sensors Journal, IEEE*, 12(5):1455–1458, May 2012.

<sup>9</sup>Charlie Strobel. *Inductive proximity sensors*. Panasonic Electric Works Corp., Newark, NJ, 2012.

<sup>10</sup>Pepperl+Fuchs Inc., Twinsburg, OH. *Sensors and systems*, 2012.

<sup>11</sup>Larry K. Baxter. *Capacitive sensors: Design and applications*. IEEE Press, New York, 1997.

<sup>12</sup>Jacob Fraden. *Handbook of modern sensors: physics, designs, and applications*. Springer, New York, 2004.

<sup>13</sup>Yann LeFaou Keith Edwin Curtis and Fanie Duvenhage. *Capacitive/inductive proximity detection for wi-fi protection*, 2013.

<sup>14</sup>Jiangtao Huangfu, Lixin Ran, Hongsheng Chen, Xian-min Zhang, Kangsheng Chen, Tomasz M. Grzegorzcyk, and Jin Au Kong. Experimental confirmation of negative refractive index of a metamaterial composed of  $\Omega$ -like metallic patterns. *Applied Physics Letters*, 84(9):1537–1539, 2004.

<sup>15</sup>Haifei Zhang, Jiangtao Huangfu, Dongxing Wang, Hongsheng Chen, Tao Peng, Lixin Ran, and Jin Au Kong. Experimental study of the hybridizing effect of different left-handed metamaterials. *Physics Letters A*, 363(5):492 – 496, 2007.

<sup>16</sup>Analog Device Inc. *Datasheet AD8302*, 2002.

<sup>17</sup>AutomationDirect Inc., Cumming, GA. *Proximity Sensor Selection Guide*.

<sup>18</sup>Omron Scientific Technologies Inc., Fremont, CA. *Omron Solution Selection Guide 2014*.

<sup>19</sup>Ifm Efector Inc., Exton, PA. *Sensors and Controls Catalog – 2013/2014*.

<sup>20</sup>SICK Sensor Intelligence Inc., Minneapolis, MN. *Top Products from SICK*.